CrossMark

The Quest for a Plausible Formation Route of Formyl Cyanide in the Interstellar Medium: a State-of-the-art Quantum-chemical and Kinetic Approach

Francesca Tonolo[1,2] , Jacopo Lupi[1] , Cristina Puzzarini[2] , and Vincenzo Barone[1]

[1] Scuola Normale Superiore, Piazza dei Cavalieri 7, Pisa, I-56126, Italy; vincenzo.barone@sns.it
[2] Department of Chemistry "Giacomo Ciamician", University of Bologna, Via F. Selmi 2, Bologna, I-40126, Italy; cristina.puzzarini@unibo.it
Received 2020 May 25; revised 2020 July 11; accepted 2020 July 13; published 2020 September 3

Abstract

Interstellar complex organic molecules are assumed to be mainly formed on dust–grain surfaces. However, neutral gas-phase reactions in the interstellar medium can play an important role. In this paper, by investigating the reaction between aldehydes and the cyano radical, we show that both formaldehyde (CH_2O) and acetaldehyde (CH_3CHO) can lead to the formation of formyl cyanide (HCOCN). Owing to accurate quantum-chemical computations followed by rate constant evaluations, we have been able to suggest and validate an effective mechanism for the formation of HCOCN, one of the molecules observed in the ISM. Quite interestingly, the mechanism starting from CH_2O is very effective at a low temperature, while that involving CH_3CHO becomes more efficient at temperatures above 200 K.

Unified Astronomy Thesaurus concepts: Interstellar medium (847); Interstellar clouds (834); Computational methods (1965); Interstellar molecules (849); Reaction rates (2081); Astrochemistry (75)

1. Introduction

In the last 50 yr more than 200 molecular species have been identified in the interstellar medium (ISM) mostly thanks to their rotational signatures (McGuire 2018). Among them, the so-called interstellar complex organic molecules (iCOMs), namely molecules containing at least one carbon atom and, overall, more than five atoms, are particularly significant because they include several precursors of biomolecule building blocks (Chyba & Sagan 1992; Herbst & van Dishoeck 2009; Balucani 2012; Hörst et al. 2012; Saladino et al. 2012, 2015).

The most widespread investigated reactions to form iCOMs are based on grain-surface chemistry because radical species trapped in icy mantles can easily react and give rise to a rich chemistry (see, e.g., Garrod & Herbst 2006; Garrod et al. 2008; Öberg et al. 2010; Linnartz et al. 2015; Rimola et al. 2018). However, the recent observation of iCOMs also in very cold objects, has suggested that the role of gas-phase reactions could have been overlooked (see, e.g., Bacmann et al. 2012; Vasyunin & Herbst 2013; Vastel et al. 2014; Balucani et al. 2015). The extreme conditions of the ISM (i.e., very low temperatures and very low density) pose strong limitations on the feasibility of chemical reactions in the gas phase, thus requiring that all transition states are submerged with respect to reactants' energy. This gives rise to a chemistry sensibly different from the conventional reactivity, under terrestrial conditions, we were used to. As a consequence, the formation pathways of the detected molecules in the typically cold and (largely) collision-free environment of the ISM are often unknown. Aiming at their disclosure and understanding, new reaction mechanisms need to be investigated from both thermochemical and kinetic points of view. While energetic studies allow for deriving possible accessible pathways, only the determination of accurate reaction rates can confirm which formation routes can indeed occur. These in turn provide useful information in view of rationalizing the molecular abundances observed in interstellar clouds.

Among the most plausible gas-phase mechanisms, radical–neutral reactions play a central role and, among them, the addition of the cyano radical (CN) to electrophilic sites is gaining an increasing interest because it might lead to the formation of compounds containing the CN moiety. The interest on the latter species is due to the fact that they can be key intermediates in the synthesis of aminoacids, the building blocks of proteins, and/or nucleobases, the essential components of nucleic acids (Vastel et al. 2014; Balucani et al. 2015; Puzzarini & Barone 2020; Salta et al. 2020).

Despite the fact that the required spectroscopic parameters of formyl cyanide (HCOCN) were available since 1995 (Bogey et al. 1995), its first and only detection in the ISM is quite recent (Remijan et al. 2008). In 2008, Remijan et al. (2008) indeed detected some of its rotational transitions toward the star-forming region Sagittarius B2(N) using the 100 m Green Bank Telescope. In spite of several spectroscopic studies carried out on HCOCN and some studies on its formation in the ISM (see Das et al. 2013 and references therein), to the best of our knowledge, an accurate investigation of possible gas-phase formation pathways has not been carried out yet. This prompted us to try to fill this lack.

The choice of possible precursors for the derivation of a gas-phase formation pathway for formyl cyanide was guided by assumptions related to the physical conditions and molecular abundances of Sagittarius B2(N). Among the various possibilities, the attack of the CN radical to formaldehyde seems to be particularly promising. Indeed, both these molecular species are widely spread in the ISM and their abundance in the Sagittarius B2 nebula qualifies them as excellent candidates (Mehringer et al. 1995; Savage et al. 2002). Furthermore, we extended such an investigation by replacing formaldehyde with acetaldehyde in the reaction with CN, whose widespread presence in the ISM, and in particular in the Sagittarius B2 nebula (Matthews et al. 1985), makes this second approach appealing as well.

The manuscript is organized as follows. First, the essential computational details for both the energetic and kinetic study are provided. In the subsequent section, the results are reported and analyzed in detail. The outcomes for the investigation of
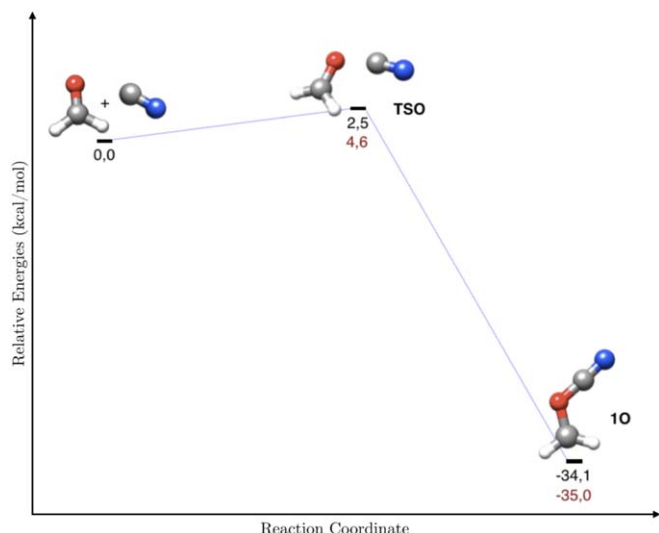
Figure 1. Reaction path of CN + CH₂O for the attack of the CN radical on the oxygen side: relative electronic B2PLYP/maug-cc-pVTZ-*d*H (black) and harmonic ZPE-corrected (dark-red) energies are reported.

the reaction of formaldehyde and acetaldehyde with the CN radical are first presented from a thermochemical point of view. Then, kinetic results for both reactions are discussed. Finally, concluding remarks are provided.

2. Computational Methodology

The starting point for the study of the formation of HCOCN is the identification of the potential reactants and the analysis of the corresponding reactive potential energy surface (PES), which implies the characterization of all stationary points from both a structural and energetic point of view. The accurate thermochemical characterization requires then to be followed by kinetic calculations. In the following the essential details are provided, while a deeper account is given in the Appendix.

As mentioned above, the physical conditions of the ISM are extreme: low temperatures (10–100 K) and low density ($10–10^7$ particles cm^{-3}). By translating density in terms of pressure, a density of 10^4 particles cm^{-3} corresponds to a pressure of 3.8×10^{-10} Pa ($\sim 3.8 \times 10^{-15}$ atm). Therefore, in the investigation of the reactions between formaldehyde or acetaldehyde with CN we take such constraints into considerations.

2.1. Reactive PES

This type of study requires the application of different levels of theory that combine accuracy and efficiency. Indeed, a preliminary investigation of the reactive PES is carried out at an affordable computational cost, thus leading to the evaluation of all possible reaction paths. Then, a structural and energetic characterization of the most favored paths is performed at a higher level of theory.

The approach followed is that employed in Vazart et al. (2016) for the gas-phase formation route of formamide and consists of the following steps:

 (i) The reactive PES has been first of all studied using a cost effective level of theory in order to locate the stationary points. The hybrid B3LYP functional (Becke 1993;

Lee et al. 1988) in conjunction with a double-ζ quality basis set (SNSD; Barone et al. 2008) has been employed, with dispersion effects taken into account (D3BJ; Grimme et al. 2010, 2011).

 (ii) To obtain a more accurate description of these pathways, all stationary points have been re-investigated at a higher level of theory using the double-hybrid B2PLYP functional (Grimme 2006) (combined with D3BJ corrections) in conjunction with a triple-ζ quality basis set incorporating diffuse functions (maug-cc-pVTZ-*d*H; Papajak et al. 2009; Fornaro et al. 2016).

 (iii) To further improve the energy determination of the stationary points of the most energetically favored paths, single-point energy calculations, at the B2PLYP/maug-cc-pVTZ-*d*H geometries, have been performed by means of the so-called CCSD(T)/CBS+CV composite scheme (Heckert et al. 2006; Puzzarini 2011; Barone et al. 2013), which is based on coupled-cluster (CC) theory and is explained in the Appendix. Finally, CCSD(T)/CBS+CV energies have been combined with anharmonic zero-point energy (ZPE) corrections evaluated at the B2PLYP/maug-cc-pVTZ-*d*H level, as detailed in the Appendix.

2.2. Kinetic Models

For both CH₂O + CN and CH₃CHO + CN reactions, global rate constants have been calculated by using a master equation (ME) approach based on ab initio transition state theory (AITSTME), thereby employing the MESS software as an ME solver (Georgievskii et al. 2013). For elementary reactions involving a transition state, rate constants have been computed using transition state theory, while for barrierless elementary reactions, they have been evaluated by means of phase space theory (PST; Pechukas & Light 1965; Chesnavich 1986). Tunneling has been accounted for using the Eckart model (Eckart 1930). A more detailed account is provided in Appendix B.

3. Results and Discussion

In Section 3.1, the results for the reactive PES of CH₂O + CN are reported and discussed, mainly focusing on the energetically favored paths. Subsequently, the analogous investigation on the reaction between acetaldehyde and CN is detailed in Section 3.2. The outcomes of the kinetic study for both reactions are reported and discussed in Section 3.3.

3.1. Mechanistic Study: CN + Formaldehyde

The examined reaction paths include:

 (i) the nucleophilic attack by carbon-CN on the carbonyl oxygen;
 (ii) the nucleophilic attack of the CN radical (both C-approach and N-approach) on the carbonyl carbon of formaldehyde;
 (iii) the abstraction of a hydrogen atom of formaldehyde by the CN radical.

As expected, the radical attacks on the carbonyl carbon site are more favorable than those on oxygen because of their different electrophilicity; in addition, the CN radical attacks preferentially by the carbon side where the unpaired electron is more localized. For these reasons, the N-attack by the CN radical on
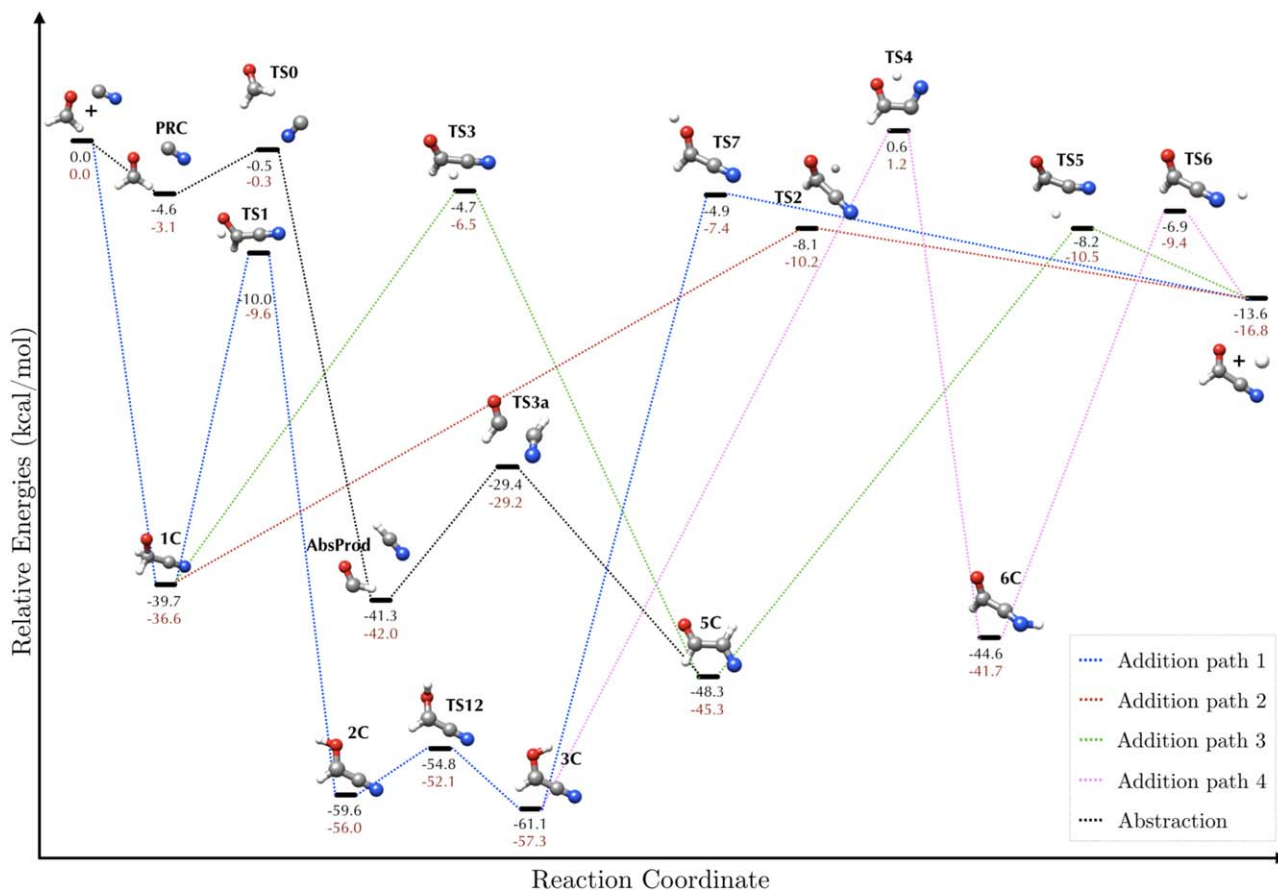
Figure 2. Formation route of formyl cyanide from the C-attack of the CN radical on the carbon side of CH$_2$O: relative CCSD(T)/CBS+CV (black) single-point energies and anharmonic ZPE-corrected (dark-red) energies are reported.

oxygen of formaldehyde is so unfavorable that it does not even occur. Likewise, the C-attack by CN on the oxygen atom of formaldehyde would lead to the formation of a single product, shown in Figure 1, through a transition state at higher energy than the reactants, which cannot be overcome in the typical conditions of the ISM. Therefore, this pathway has not been further considered.

Figure 2 shows the reaction paths derived for the C-attack of the CN radical on formaldehyde and the abstraction of a hydrogen atom of formaldehyde by the CN radical. These pathways are those of interest because they can lead to the formation of the sought product only requiring submerged barriers (i.e., lower in energy with respect to reactants) to be overcome.

The first molecular species formed from the interaction between the two reactants, is the tetrahedral intermediate 1C, which is energetically favored by about 40 kcal mol^{-1} and can lead to the desired products overcoming the transition state TS2 (see red path). This path is particularly interesting from an energetic point of view because it yields formyl cyanide by passing through the least number of intermediates and transition states. The intermediate 1C can also lead to the formation of the two isomers 2C and 3C which, being the most stable intermediates of the investigated reactive PES, could be competitive with the formation of formyl cyanide. The same is the case for the green path, which is also favored from an

Table 1
Relative Electronic Energies (in kcal mol^{-1}) of the Stationary Points Shown in Figure 2, Calculated at the B2PLYP/maug-cc-pVTZ-dH and CCSD(T)/CBS +CV Levels of Theory, also Including Anharmonic ZPE Corrections

	B2PLYP/ maug-cc-pVTZ-dH		CCSD(T)/ CBS+CV	
	Energy	ZPE Corrected	Energy	ZPE Corrected
CH$_2$O + CN	0.0	0.0	0.0	0.0
1C	−41.1	−38.0	−39.7	−36.6
PRC	−7.1	−5.4	−4.6	−3.1
TS1	−11.5	−11.1	−10.0	−9.6
TS0	−0.8	−0.5	−0.5	−0.3
AbsProd	−43.2	−43.8	−41.3	−42.0
2C	−60.8	−57.2	−59.6	−56.0
TS12	−55.7	−53.0	−54.8	−52.1
3C	−62.4	−58.6	−61.1	−57.3
TS3	−7.4	−9.2	−4.7	−6.5
TS3a	−32.3	−31.9	−29.4	−29.2
5C	−49.8	−46.7	−48.3	−45.3
TS7	−8.3	−10.8	−4.9	−7.4
TS2	−10.4	−12.5	−8.1	−10.2
TS4	−1.3	−0.7	0.6	1.2
6C	−48.2	−45.3	−44.6	−41.7
TS5	−10.3	−12.6	−8.2	−10.5
TS6	−10.6	−13.0	−6.9	−9.4
HCOCN+H	−15.3	−18.5	−13.6	−16.8

3
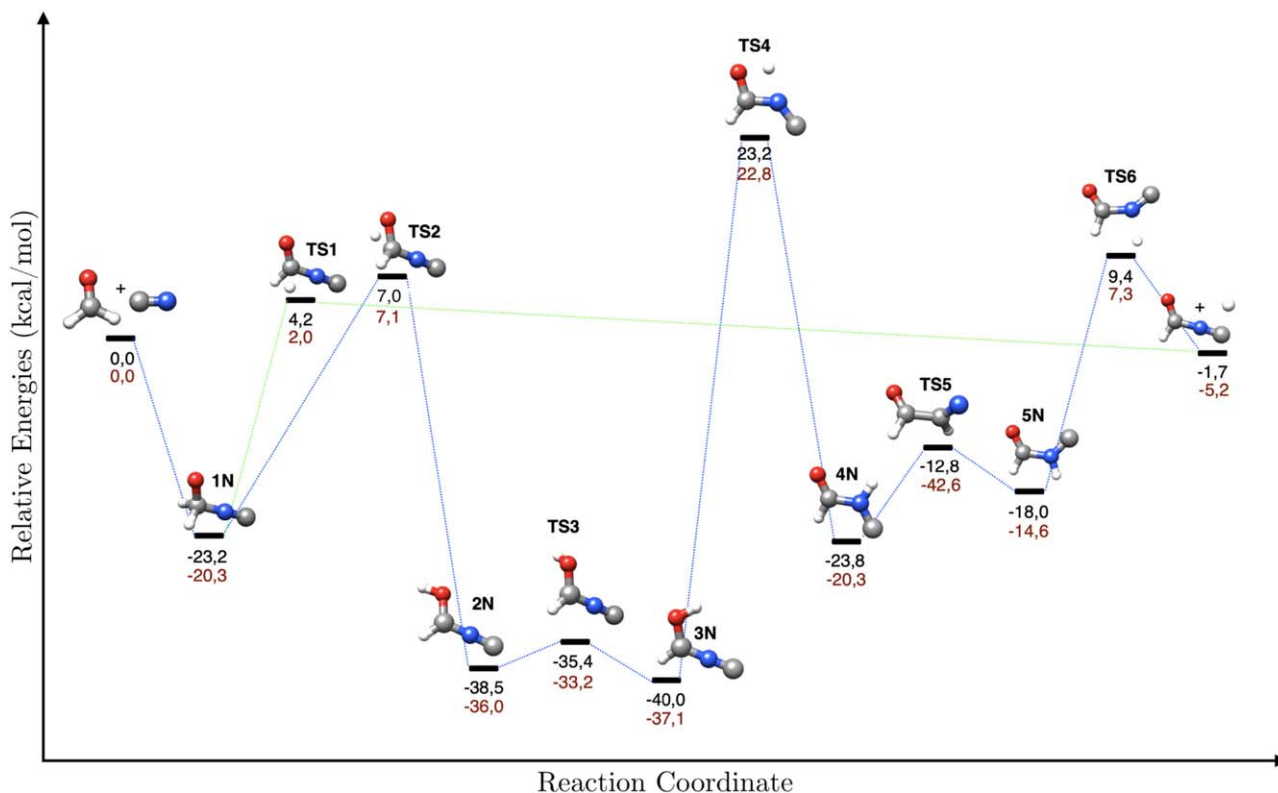
Figure 3. Reaction path of the reaction CN + CH$_2$O → HCONC + H for the attack of the CN radical on the nitrogen side: relative electronic B2PLYP/maug-cc-pVTZ-*d*H (black) and harmonic ZPE-corrected (dark red) energies are reported.
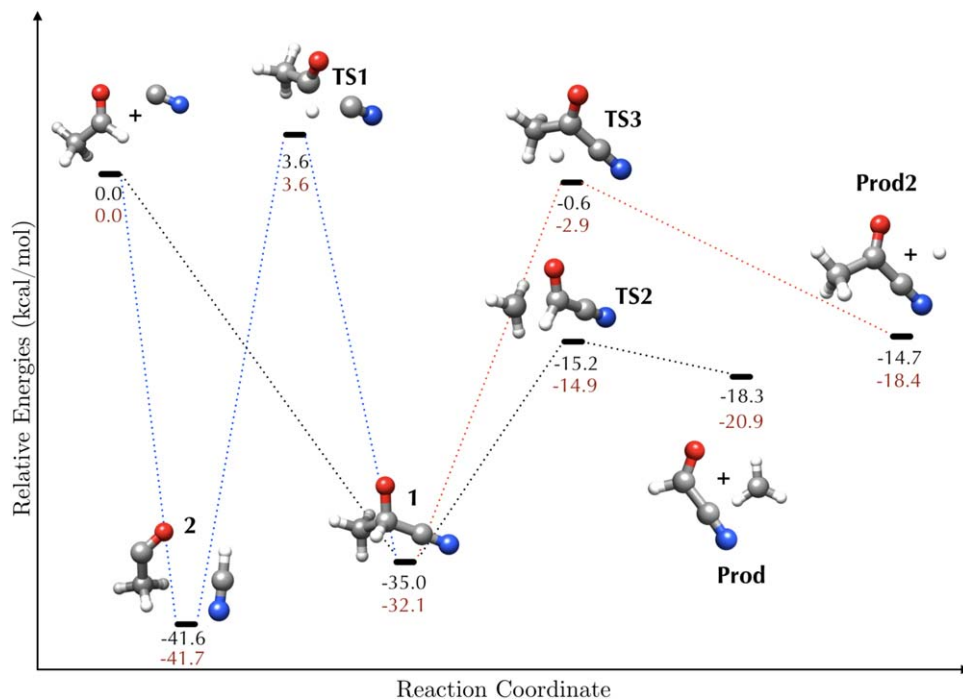
Figure 4. Formation route of formyl cyanide from the C-attack of the CN radical on the carbon side of CH$_3$CHO: relative CCSD(T)/CBS+CV (black) single-point energies and anharmonic ZPE-corrected (dark-red) energies are reported.

energetic point of view, but it might represent a kinetic sink for the sought reaction. The path represented in pink is ruled by a transition state (TS4) lying at an energy very close to that of the

reactants. Therefore, this path is not very favorable under the ISM conditions. Finally, the black path involves the abstraction of a hydrogen of formaldehyde by the CN radical: a

Table 2
Relative Electronic Energies (in kcal mol^{-1}) of the Stationary Points Shown in Figure 4, Calculated at the B2PLYP/maug-cc-pVTZ-dH and CCSD(T)/CBS+CV Levels of Theory, also Including Anharmonic ZPE Corrections

	B2PLYP/ maug-cc-pVTZ-dH		CCSD(T)/ CBS+CV	
	Energy	ZPE Corrected	Energy	ZPE Corrected
CH$_3$COH + CN	0.0	0.0	0.0	0.0
1	−35.7	−32.8	−35.0	−32.1
2	−43.5	−43.5	−41.6	−41.7
TS1	−0.3	−0.4	3.6	3.6
TS2	−18.0	−17.8	−15.2	−14.9
HCOCN + CH$_3$	−20.4	−23.1	−18.3	−20.9
TS3	−8.8	−11.1	−0.6	−2.9
CH$_3$COCN + H	−16.2	−19.9	−14.7	−18.4

pre-reactive complex (PRC) is formed, and then the abstraction occurs. After overcoming the transition state TS0, PRC leads to the formation of HCN and the formyl radical (HCO), denoted as AbsProd. The transition state TS0 is slightly more stable than the reactants also at higher levels of theory (vide infra). Once the AbsProd are formed, they can further react to give the intermediate 5C *via* the transition state TS3a, thus leading to the formation of formyl cyanide along the green path. The involvement of these intermediates in further chemical transformations would be probably possible only via a roaming mechanism (Bowman & Zhang 2006; Suits 2008). However, in view of the large excess of energy and the high barrier for the subsequent transition state relative to the abstraction products (TS3a), the contribution of this channel to the overall reaction is negligible.

From an energetic point of view, the various pathways of Figure 2 are open even in the harsh conditions of the ISM. For this reason, they have been investigated at a higher level of theory (CCSD(T)/CBS+CV), the results being reported in Table 1. While this composite scheme does not change the trends resulting from B2PLYP calculations, it reduces the relative energies with respect to the reactants. This leads to intermediates that are less stable by about 1–3 kcal mol^{-1}, which often means small energy barriers to be overcome. Based on the available literature (see, e.g., Puzzarini 2011; Barone et al. 2013; Puzzarini & Barone 2020), the CCSD(T)/CBS+CV approach improves the expected accuracy, thus reducing the error bars on relative energies below 0.5 kcal mol^{-1}.

The last mechanism considered for the reaction between CN and CH$_2$O is the N-attack of CN on the carbon side of formaldehyde, which is shown in Figure 3. All the possible paths issuing from this approach involve transition states at higher energy than the reactants, thus preventing the reaction to occur in the typical conditions of the ISM.

3.2. Mechanistic Study: CN + Acetaldehyde

As mentioned in the Introduction, another mechanism investigated for the formation of formyl cyanide is the reaction between acetaldehyde and the CN radical. Figure 4 shows the corresponding reactive PES.

The path identified in black represents the direct attack of CN on the carbonyl carbon of acetaldehyde. In analogy to the CH$_2$O + CN reaction, this attack leads to the formation of a tetrahedral intermediate (1), from which both formyl cyanide

and acetyl cyanide (red path) can be obtained. Since the formation of both products involves only submerged barriers, the corresponding paths are feasible from an energetic point of view in the conditions of the ISM. Furthermore, it is interesting that formyl cyanide is the favored product from an energetic point of view. The path traced in blue describes the abstraction of a hydrogen atom of acetaldehyde by the CN radical. This leads to the formation of HCN and the acetyl radical (CH$_3$CO), which can further react and form the tetrahedral intermediate 1 through the transition state TS1. In analogy to the hydrogen abstraction path of the CH$_2$O + CN reaction, roaming mechanisms might play a role (Bowman & Zhang 2006; Suits 2008). However, as above, the large excess of energy and the high barrier due to TS1 are expected to provide a negligible contribution.

As already discussed for CH$_2$O + CN, for all stationary points, improved energies have been obtained by single-point CCSD(T)/CBS+CV computations at B2PLYP/maug-cc-pVTZ-dH reference geometries. The corresponding results, collected in Table 2, confirm the overall picture provided by B2PLYP energies. However, it is noteworthy that the energy of TS1 at such level of theory is higher than that of the reactants, thus preventing the H abstraction to occur in the typical conditions of the ISM. As a general note, a brief comment on the comparison of B2PLYP and CCSD(T)/CBS+CV energies is deserved. For all the stationary points characterizing the addition of CN to formaldehyde, the maximum and average absolute errors of B2PLYP results with respect to CCSD(T)/CBS+CV values are 3.8 and 2.1 kcal mol^{-1}, respectively. Moving to the addition to acetaldehyde, the deviations remain similar, i.e., 3.7 and 1.7 kcal mol^{-1}, respectively. Overall, the B2PLYP/maug-cc-pVTZ-dH level leads to errors about two to four times larger than those expected for the CCSD(T)/CBS+CV approach.

3.3. Rate Coefficients

According to the results discussed in the two preceding sections, the reactive PES for the formation of formyl cyanide from CH$_3$CHO and CN involves intermediates that are, in the majority of the cases, energetically less stable than those of the CH$_2$O + CN PES. Therefore, a kinetic study is mandatory, not only to evaluate the specific (and global) rate constants, but also to understand whether:

(i) the presence of particularly stable intermediates in the CH$_2$O + CN reaction might represent a kinetic sink;
(ii) both reactions are effective and/or which one is more efficient;
(iii) concerning point (ii), the temperature plays a role.

Global and channel specific rate constants for the CH$_2$O + CN and CH$_3$CHO + CN reactions have been computed, as described in Section 2.2, using the PESs depicted in Figures 2 and 4. The multi-well one-dimensional ME has been solved by exploiting the chemically significant eigenvalues (CSEs) method within the Rice–Ramsperger–Kassel–Marcus (RRKM) approximation, as detailed in Miller & Klippenstein (2006). All rate coefficients have been computed in the 30–300 K temperature range and at pressure of 1×10^{-12} atm. The temperature dependence plots are shown in Figures 5 (channel rates) and 6 (global rate) for the formaldehyde + CN reaction, and in Figure 7 for the acetaldehyde + CN reaction.
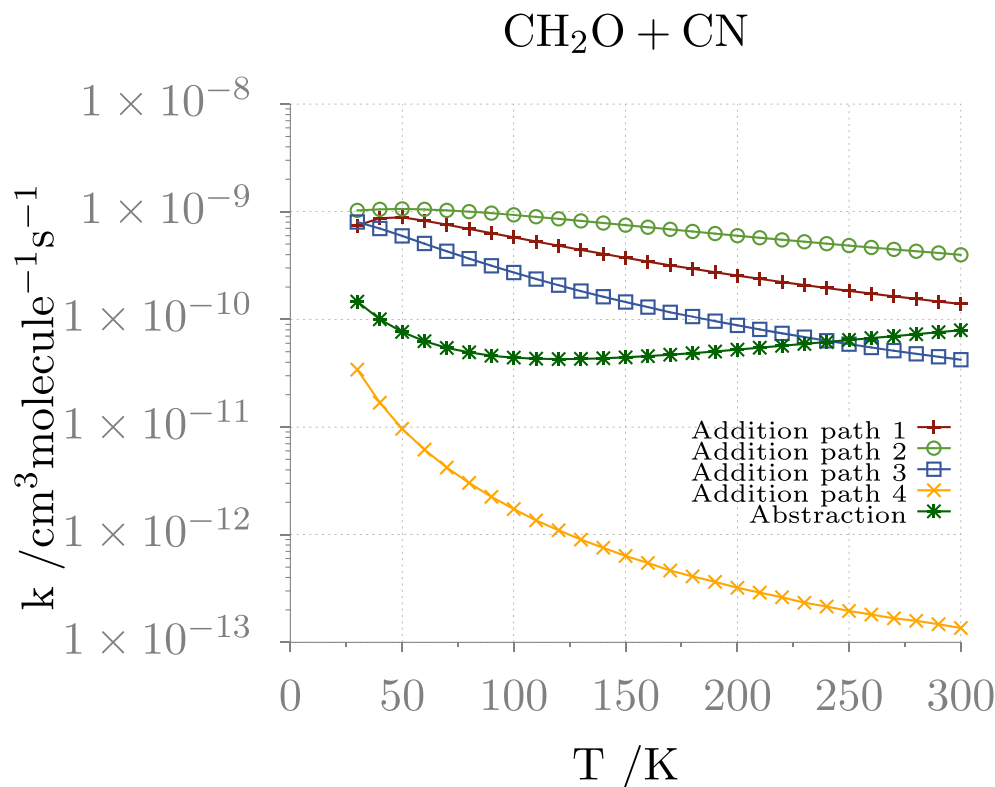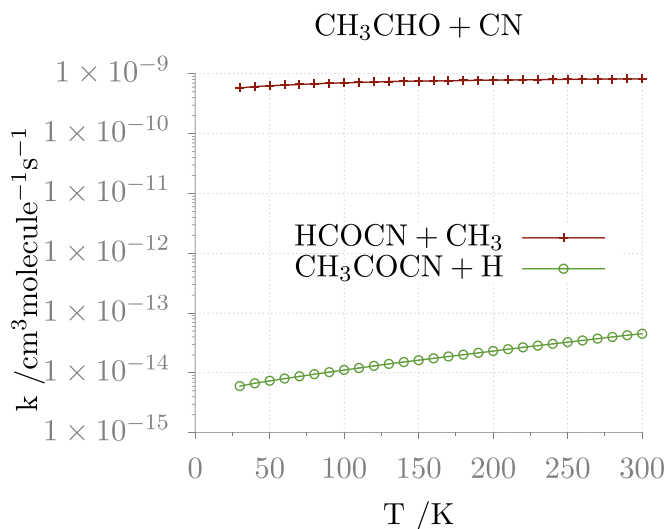
Figure 5. Channel specific rate constants for the $CH_2O + CN$ reaction leading to $HCOCN + H$.
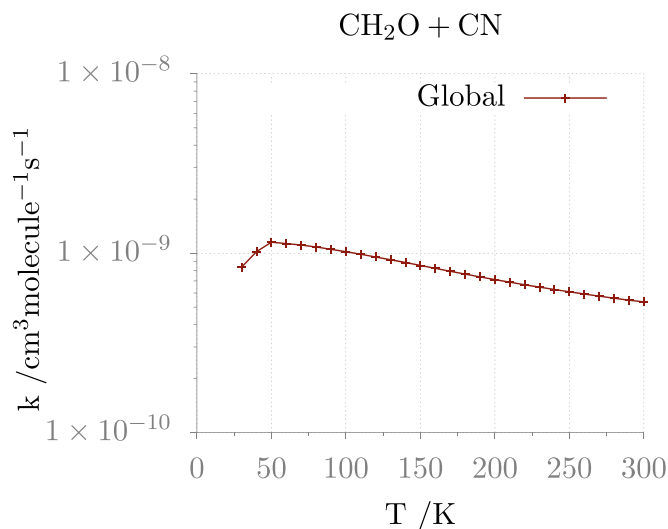
Figure 6. Global rate constant for $CH_2O + CN$ reaction.

Figure 7. Rate constants for the $CH_3CHO + CN$ reaction leading to $HCOCN + CH_3$ and $CH_3COCN + H$.

For these calculations, the CCSD(T)/CBS+CV energies, corrected by anharmonic ZPE values, have been employed for reaction paths involving a nonnegligible transition state, while rate constants of the barrierless channels have been computed using PST (see Section 2.2 and Appendix B). The uncertainty on reaction rates issuing from the errors in the computed CCSD(T)/CBS+CV energies is below 20%, which is largely sufficient for the comparison with the experiment. Reaction rates computed with B2PLYP energies are within a factor of 2 from their CCSD(T)/CBS+CV counterparts in the whole

range of temperatures between 50 and 300 K, except for product P2 in the acetaldehyde reaction (due to a much lower activation energy of the key step). However, since this product is negligible, the agreement is quite reasonable.

Within the temperature interval considered, for the $CH_2O + CN$ reaction, the fastest reaction channel is always the addition path 2 (see Figure 2 for path labeling), though the relevance of the abstraction path is nonnegligible, its rate constant differing by less than one order of magnitude with respect to that of path 2. Regarding to the $CH_3CHO + CN$ reaction, as expected,

Table 3
Product-formation Rate Constants (in cm^3 molecule^{-1} s^{-1}) at 1×10^{-12} atm as a Function of Temperature

	Formaldehyde						Acetaldehyde	
T (K)	Path 1	Path 2	Path 3	Path 4	Abstraction	Global	HCOCN + CH$_3$	CH$_3$COCN + H
30	7.42×10^{-10}	1.03×10^{-09}	8.04×10^{-10}	3.42×10^{-11}	1.46×10^{-10}	8.35×10^{-10}	5.81×10^{-10}	6.03×10^{-15}
40	8.70×10^{-10}	1.05×10^{-09}	6.99×10^{-10}	1.68×10^{-11}	1.00×10^{-10}	1.02×10^{-09}	6.10×10^{-10}	6.70×10^{-15}
50	8.86×10^{-10}	1.06×10^{-09}	5.97×10^{-10}	9.63×10^{-12}	7.64×10^{-11}	1.15×10^{-09}	6.33×10^{-10}	7.37×10^{-15}
60	8.23×10^{-10}	1.05×10^{-09}	5.06×10^{-10}	6.17×10^{-12}	6.27×10^{-11}	1.13×10^{-09}	6.52×10^{-10}	8.06×10^{-15}
70	7.58×10^{-10}	1.03×10^{-09}	4.30×10^{-10}	4.21×10^{-12}	5.44×10^{-11}	1.11×10^{-09}	6.69×10^{-10}	8.78×10^{-15}
80	6.93×10^{-10}	1.00×10^{-09}	3.67×10^{-10}	3.02×10^{-12}	4.93×10^{-11}	1.08×10^{-09}	6.84×10^{-10}	9.54×10^{-15}
90	6.33×10^{-10}	9.70×10^{-10}	3.15×10^{-10}	2.25×10^{-12}	4.60×10^{-11}	1.05×10^{-09}	6.97×10^{-10}	1.03×10^{-14}
100	5.78×10^{-10}	9.34×10^{-10}	2.72×10^{-10}	1.73×10^{-12}	4.41×10^{-11}	1.02×10^{-09}	7.10×10^{-10}	1.12×10^{-14}
110	5.27×10^{-10}	8.97×10^{-10}	2.37×10^{-10}	1.36×10^{-12}	4.31×10^{-11}	9.88×10^{-10}	7.21×10^{-10}	1.21×10^{-14}
120	4.82×10^{-10}	8.60×10^{-10}	2.08×10^{-10}	1.10×10^{-12}	4.28×10^{-11}	9.54×10^{-10}	7.31×10^{-10}	1.31×10^{-14}
130	4.42×10^{-10}	8.22×10^{-10}	1.83×10^{-10}	9.01×10^{-13}	4.29×10^{-11}	9.19×10^{-10}	7.40×10^{-10}	1.41×10^{-14}
140	4.05×10^{-10}	7.86×10^{-10}	1.62×10^{-10}	7.54×10^{-13}	4.35×10^{-11}	8.86×10^{-10}	7.49×10^{-10}	1.52×10^{-14}
150	3.73×10^{-10}	7.51×10^{-10}	1.45×10^{-10}	6.34×10^{-13}	4.44×10^{-11}	8.54×10^{-10}	7.57×10^{-10}	1.63×10^{-14}
160	3.44×10^{-10}	7.17×10^{-10}	1.30×10^{-10}	5.46×10^{-13}	4.56×10^{-11}	8.23×10^{-10}	7.64×10^{-10}	1.75×10^{-14}
170	3.18×10^{-10}	6.85×10^{-10}	1.16×10^{-10}	4.65×10^{-13}	4.70×10^{-11}	7.93×10^{-10}	7.71×10^{-10}	1.88×10^{-14}
180	2.95×10^{-10}	6.54×10^{-10}	1.06×10^{-10}	4.10×10^{-13}	4.86×10^{-11}	7.65×10^{-10}	7.77×10^{-10}	2.02×10^{-14}
190	2.74×10^{-10}	6.26×10^{-10}	9.63×10^{-11}	3.64×10^{-13}	5.04×10^{-11}	7.38×10^{-10}	7.83×10^{-10}	2.17×10^{-14}
200	2.55×10^{-10}	5.98×10^{-10}	8.80×10^{-11}	3.21×10^{-13}	5.23×10^{-11}	7.13×10^{-10}	7.89×10^{-10}	2.33×10^{-14}
210	2.38×10^{-10}	5.73×10^{-10}	8.06×10^{-11}	2.90×10^{-13}	5.45×10^{-11}	6.89×10^{-10}	7.94×10^{-10}	2.49×10^{-14}
220	2.22×10^{-10}	5.48×10^{-10}	7.42×10^{-11}	2.62×10^{-13}	5.67×10^{-11}	6.67×10^{-10}	7.99×10^{-10}	2.67×10^{-14}
230	2.08×10^{-10}	5.26×10^{-10}	6.84×10^{-11}	2.33×10^{-13}	5.91×10^{-11}	6.46×10^{-10}	8.03×10^{-10}	2.86×10^{-14}
240	1.96×10^{-10}	5.04×10^{-10}	6.33×10^{-11}	2.15×10^{-13}	6.16×10^{-11}	6.27×10^{-10}	8.07×10^{-10}	3.06×10^{-14}
250	1.84×10^{-10}	4.84×10^{-10}	5.88×10^{-11}	1.96×10^{-13}	6.43×10^{-11}	6.09×10^{-10}	8.11×10^{-10}	3.27×10^{-14}
260	1.73×10^{-10}	4.65×10^{-10}	5.48×10^{-11}	1.81×10^{-13}	6.71×10^{-11}	5.92×10^{-10}	8.14×10^{-10}	3.49×10^{-14}
270	1.64×10^{-10}	4.47×10^{-10}	5.11×10^{-11}	1.67×10^{-13}	6.99×10^{-11}	5.76×10^{-10}	8.17×10^{-10}	3.73×10^{-14}
280	1.55×10^{-10}	4.30×10^{-10}	4.78×10^{-11}	1.58×10^{-13}	7.29×10^{-11}	5.61×10^{-10}	8.20×10^{-10}	3.98×10^{-14}
290	1.46×10^{-10}	4.14×10^{-10}	4.49×10^{-11}	1.47×10^{-13}	7.60×10^{-11}	5.47×10^{-10}	8.22×10^{-10}	4.25×10^{-14}
300	1.39×10^{-10}	3.98×10^{-10}	4.22×10^{-11}	1.36×10^{-13}	7.92×10^{-11}	5.35×10^{-10}	8.24×10^{-10}	4.53×10^{-14}

the dominant reaction channel at all temperatures is the one leading to HCOCN. Within the uncertainty derived from the model used for the entrance channel, the formaldehyde + CN reaction seems to be faster than the acetaldehyde + CN one in the ISM harsh conditions at least in the 30–150 K temperature range. Then, in the 150–200 K interval the global rate constants are very similar, with the reaction involving CH$_3$CHO becoming a little bit faster at temperatures above 200 K (see Table 3).

Even if of limited astrophysical interest (but of potential relevance in planetary atmospheres), it is worthwhile investigating the high-pressure limit rate constants for the interconversion of the entrance channel wells. Concerning the CH$_2$O + CN reaction, at 300 K, the addition entrance well interconverts into the products with a rate coefficient of 2.16×10^{-10} cm^3 molecule^{-1} s^{-1} and into the reactants with a rate coefficient of 1.40×10^{-6} cm^3 molecule^{-1} s^{-1}, while the abstraction entrance well never reaches in an effective way the final products, going rather back to the reactants. On the other hand, in the CH$_3$CHO + CN reaction, the entrance well interconversion toward the products largely overwhelms that back to the reactants, with rate coefficients of 2000 and 5.86×10^{-7} cm^3 molecule^{-1} s^{-1}, respectively. This leads us to conclude that, assuming that the entrance well is collisionally stabilized, formyl cyanide can be formed only by the CH$_3$CHO + CN reaction, while in the ISM extreme conditions it can be formed efficiently by both reactions, since the reaction proceeds by well-skipping.

4. Conclusions and Perspectives

The main aim of this study was the disclosure of a feasible gas-phase mechanism for the formation of formyl cyanide in the ISM. The selection of possible precursors was based on relative abundances of CN, formaldehyde, and acetaldehyde in the Sagittarius B2 region, where also formyl cyanide was detected. Guided by state-of-the-art electronic and kinetic computations, we succeeded in characterizing and validating reasonable mechanisms starting from the C-attack of the CN radical on formaldehyde as well as on acetaldehyde, and/or the abstraction of a hydrogen atom of formaldehyde by the CN radical. All the elementary steps of these reactions are ruled by energy barriers submerged with respect to reactants, thus pointing out the feasibility of HCOCN production in the extreme conditions of the ISM. The study of the reaction mechanisms starting from acetaldehyde has shown that formation of CH$_3$COCN, while being feasible, is less probable than that of HCOCN. This can be explained in terms of the greater strength of the C–H bond with respect to the C–C one.

The solution of an ME including the different reaction channels showed that the very low pressures characterizing the ISM permit to reach the final products, even in the presence of very stable intermediates (as is the case for formaldehyde), which cannot act as effective kinetic sinks. As a consequence, under these conditions, the reaction of formaldehyde is faster than that of acetaldehyde, whereas the situation is reversed at higher pressures (where collision stabilization plays a role).

Together with the intrinsic interest of the studied systems, this paper shows, in our opinion, that state-of-the-art quantum-chemical methodologies represent a very important tool for astrochemical studies when integrated with last generation kinetic models based on the ab initio ME paradigm.

Appendix A
Reactive PES: Computational Details

(i) Preliminary investigation: stationary points (minima and transition states) have been computed using the hybrid B3LYP functional (Becke 1993; Lee et al. 1988) in conjunction with SNSD basis set (Barone et al. 2008), and accounting for dispersion effects according to Grimme's D3 scheme (Grimme et al. 2010) combined with Becke–Johnson (BJ) damping function (Grimme et al. 2011). The nature of all stationary points found on the PES has been checked by diagonalizing the corresponding Hessian matrices. To correctly connect two minima through the corresponding transition state, intrinsic reaction coordinate calculations have been performed (Fukui 1981; Hratchian & Frisch 2011).

(ii) Definition of the reactive PES: all stationary points have been re-investigated at the B2PLYP/maug-cc-pVTZ-dH level (Grimme 2006; Papajak et al. 2009; Fornaro et al. 2016), always employing the D3BJ correction. At this stage, energies are corrected for the ZPE contribution within the harmonic approximation.

(iii) Final thermochemistry: the most energetically favored paths have been selected. For the corresponding stationary points, single-point energy calculations, at the B2PLYP/maug-cc-pVTZ-dH reference geometries, have been performed by means of the CCSD(T)/CBS+CV composite scheme (Heckert et al. 2006; Puzzarini 2011; Barone et al. 2013), which is based on CC theory employing the singles and doubles approximation (CCSD) augmented by a perturbative treatment of triple excitations, CCSD(T) (Watts et al. 1993; Raghavachari 2013).

The CCSD(T)/CBS+CV energy is obtained according to the following expression:

$$E_{\text{tot}} = E_{\text{HF}}^{\infty} + \Delta E_{\text{CCSD(T)}}^{\infty} + \Delta E_{\text{CV}}, \qquad (A1)$$

where the first term on the right-hand side is the Hartree–Fock self-consistent-field (HF–SCF) energy extrapolated to the complete basis set (CBS) limit (E_{HF}^{∞}) by means of the exponential extrapolation formula by Feller (Feller 1993). The second term is the extrapolation to the CBS limit of the CCSD(T) correlation energy ($\Delta E_{\text{CCSD(T)}}^{\infty}$), using the two-point n^{-3} formula by Helgaker et al. (1997). In order to exploit these extrapolative expressions, HF–SCF and CCSD(T) energy calculations have been performed using Dunning's cc-pVnZ basis sets (Dunning 1989), with $n =$ T, Q, 5 for the HF–SCF extrapolation and $n =$ T, Q for the CCSD(T) correlation energy.

The last term is the core-valence (CV) correlation energy correction (ΔE_{CV}), which is evaluated as the energy difference between all-electron and frozen-core CCSD(T) calculations in the same basis set (cc-pCVTZ; Woon & Dunning 1995). This contribution is required because the extrapolation to the CBS limit is performed within the frozen-core approximation. As mentioned in the main text, the CCSD(T)/CBS+CV energies have been combined with anharmonic B2PLYP ZPE corrections obtained within second-order vibrational perturbation theory (VPT2; Hoy et al. 1972; Mills 1972; Barone 2004). Among the various formulations, the Hybrid Degeneracy Corrected VPT2 (HDCPT2) model (Bloino et al. 2012) has been used.

Appendix B
Kinetic Calculations: Computational Details

As aforementioned in Section 2.2, barrierless channels were treated with PST. Indeed, it provides a useful, and easily implemented, reference theory for barrierless reactions. The basic assumption in PST is that the interaction between the two reacting fragments is isotropic and does not affect the internal fragment motions. This assumption is only valid if the dynamical bottleneck lies at large separations where the interacting fragments have free rotations and unperturbed vibrations, which is generally true for low temperature phenomena as those occurring in the ISM. The isotropic potential is assumed to be described by the functional form $-\frac{C}{R^6}$, where the coefficient C is obtained by fitting the energies obtained at various long-range distances of fragments. The latter were obtained using the double-hybrid B2PLYP functional in conjunction with the maug-cc-pVTZ-dH basis set and incorporating dispersion corrections (D3BJ as already mentioned above). The C coefficients were then corrected in order to obtain entrance channels rate constant values scaled by a 0.9 factor (in analogy to what is done in Georgievskii & Klippenstein 2003), which is a dynamical correction factor that takes into account the recrossing effects. The final values for the C are 290.79, 443.34 and 506.68 $a_0^6 E_{\text{h}}$, for the formaldehyde addition, formaldehyde abstraction and acetaldehyde addition, respectively. To check the role of the basis set superposition error in the evaluation of the PST coefficient, counterpoise (CP) corrected long-range electronic energies have been computed at various interfragment distances, thereby leading to a small difference of ca. 3 $a_0^6 E_{\text{h}}$ with respect to the non-CP corrected values. Such a small difference is essentially nonrelevant for the calculation of the entrance reactive flux, thus allowing to safely use non-CP corrected energies.

In Table 3, the channel specific and global rate constants are collected.

Appendix C
Software Packages

All DFT and VPT2 calculations have been carried out with the Gaussian software (Frisch et al. 2016), while for those based on CCSD(T) the CFOUR program[3] (Matthews et al. 2020) has been employed. RRKM simulations have been performed with eMESS code (Georgievskii et al. 2013), available at https://github.com/PACChem/MESS.

---

[3] http://www.cfour.de

ORCID iDs

Francesca Tonolo ⓘ https://orcid.org/0000-0002-9555-7834
Jacopo Lupi ⓘ https://orcid.org/0000-0001-6522-9947
Cristina Puzzarini ⓘ https://orcid.org/0000-0002-2395-8532
Vincenzo Barone ⓘ https://orcid.org/0000-0001-6420-4107

References

Bacmann, A., Taquet, V., Faure, A., Kahane, C., & Ceccarelli, C. 2012, A&A, 541, L12
Balucani, N. 2012, Chem. Soc. Rev., 41, 5473
Balucani, N., Ceccarelli, C., & Taquet, V. 2015, MNRAS, 449, L16
Barone, V. 2004, JChPh, 120, 3059
Barone, V., Biczysko, M., Bloino, J., & Puzzarini, C. 2013, PCCP, 15, 10094
Barone, V., Cimino, P., & Stendardo, E. 2008, J. Chem. Theory Comput., 4, 751
Becke, A. D. 1993, JChPh, 98, 5648
Bloino, J., Biczysko, M., & Barone, V. 2012, J. Chem. Theory Comput., 8, 1015
Bogey, M., Demuynck, C., Destombes, J., & Vallee, Y. 1995, JMoSp, 172, 344
Bowman, J. M., & Zhang, X. 2006, PCCP, 8, 321
Chesnavich, W. J. 1986, JChPh, 84, 2615
Chyba, C., & Sagan, C. 1992, Natur, 355, 125
Das, A., Majumdar, L., Chakrabarti, S. K., Saha, R., & Chakrabarti, S. 2013, MNRAS, 433, 3152
Dunning, T. H., Jr. 1989, JChPh, 90, 1007
Eckart, C. 1930, PhRv, 35, 1303
Feller, D. 1993, JChPh, 7059
Fornaro, T., Biczysko, M., Bloino, J., & Barone, V. 2016, PCCP, 18, 8479
Frisch, M. J., Trucks, G. W., Schlegel, H. B., et al. 2016, Gaussian 16, Revision C.01 (Wallingford, CT: Gaussian Inc.), https://gaussian.com/citation/
Fukui, K. 1981, Acc. Chem. Res., 14, 363
Garrod, R. T., & Herbst, E. 2006, A&A, 457, 927
Garrod, R. T., Weaver, S. L. W., & Herbst, E. 2008, ApJ, 682, 283
Georgievskii, Y., & Klippenstein, S. J. 2003, JChPh, 118, 5442
Georgievskii, Y., Miller, J. A., Burke, M. P., & Klippenstein, S. J. 2013, JPCA, 117, 12146
Grimme, S. 2006, JChPh, 124, 034108
Grimme, S., Antony, J., Ehrlich, S., & Krieg, H. 2010, JChPh, 132, 154104
Grimme, S., Ehrlich, S., & Goerigk, L. 2011, JCoCh, 32, 1456
Heckert, M., Kállay, M., Tew, D. P., Klopper, W., & Gauss, J. 2006, JChPh, 125, 044108
Helgaker, T., Klopper, W., Koch, H., & Noga, J. 1997, JChPh, 106, 9639
Herbst, E., & van Dishoeck, E. F. 2009, ARA&A, 47, 427
Hörst, S., Yelle, R., Buch, A., et al. 2012, AsBio, 12, 809
Hoy, A. R., Mills, I. M., & Strey, G. 1972, MolPh, 24, 1265
Hratchian, H. P., & Frisch, M. J. 2011, JChPh, 134, 204103
Lee, C., Yang, W., & Parr, R. G. 1988, PhRvB, 37, 785
Linnartz, H., Ioppolo, S., & Fedoseev, G. 2015, IRPC, 34, 205
Matthews, D. A., Cheng, L., Harding, M. E., et al. 2020, JChPh, 152, 214108
Matthews, H. E., Friber, P., & Irvine, W. M. 1985, ApJ, 290, 609
McGuire, B. A. 2018, ApJS, 239, 17
Mehringer, D. M., Palmer, P., & Goss, W. M. 1995, ApJS, 97, 497
Miller, J. A., & Klippenstein, S. J. 2006, JPCA, 110, 10528
Mills, I. M. 1972, in Molecular Spectroscopy: Modern, ed. K. N. Rao & C. W. Matthews (New York: Academic Press)
Öberg, K. I., Bottinelli, S., Jørgensen, J. K., & van Dishoeck, E. F. 2010, ApJ, 716, 825
Papajak, E., Leverentz, H. R., Zheng, J., & Truhlar, D. G. 2009, J. Chem. Theory Comput., 5, 1197
Pechukas, P., & Light, J. C. 1965, JChPh, 42, 3281
Puzzarini, C. 2011, PCCP, 13, 21319
Puzzarini, C., & Barone, V. 2020, PCCP, 22, 6507
Raghavachari, K. 2013, CPL, 589, 35
Remijan, A. J., Hollis, J. M., Lovas, F. J., et al. 2008, ApJ, 675, L85
Rimola, A., Skouteris, D., Balucani, N., et al. 2018, ESC, 2, 720
Saladino, R., Botta, G., Pino, S., Costanzo, G., & Di Mauro, E. 2012, Chem. Soc. Rev., 41, 5526
Saladino, R., Carota, E., Botta, G., et al. 2015, PNAS, 112, E2746
Salta, Z., Tasinato, N., Lupi, J., et al. 2020, ESC, 4, 774
Savage, C., Apponi, A. J., Ziurys, L. M., & Wyckoff, S. 2002, ApJ, 578, 211
Suits, A. G. 2008, Acc. Chem. Res., 41, 873
Vastel, C., Ceccarelli, C., Lefloch, B., & Bachiller, R. 2014, ApJ, 795, L2
Vasyunin, A. I., & Herbst, E. 2013, ApJ, 769, 34
Vazart, F., Calderini, D., Puzzarini, C., Skouteris, D., & Barone, V. 2016, J. Chem. Theory Comput., 12, 5385
Watts, J. D., Gauss, J., & Bartlett, R. J. 1993, JChPh, 98, 8718
Woon, D. E., & Dunning, T. H., Jr. 1995, JChPh, 103, 4572